


# An adjustment-free laser resonator based on micron-scale corner cube array

Pengyuan Chang(常鹏媛), Xinrong Huang(黄欣荣), Caolei Fu(傅曹雷), Aiping Liu(刘爱萍), Duo Pan(潘多), Zhiyang Wang(王志洋), and Jingbiao Chen(陈景标)

**Citation:**Chin. Phys. B, 2025, 34 (**3**): 034201. DOI: 10.1088/1674-1056/ada434
Journal homepage: http://cpb.iphy.ac.cn; http://iopscience.iop.org/cpb

**What follows is a list of articles you may be interested in**

---

## High peak power mini-array quantum cascade lasers operating in pulsed mode

Yuhang Zhang(章宇航), Yupei Wang(王渝沛), Xiaoyue Luo(罗晓玥), Chenhao Qian(钱晨灏), Yang Cheng(程洋), Wu Zhao(赵武), Fangyuan Sun(孙方圆), Jun Wang(王俊), and Zheng-Ming Sun(孙正明)

Chin. Phys. B, 2025, 34 (**1**): 014204. DOI: 10.1088/1674-1056/ad886b

## Tunable artificial plasmonic nanolaser with wide spectrum emission operating at room temperature

Peng Zhou(周鹏), Jia-Qi Guo(郭佳琦), Kun Liang(梁琨), Lei Jin(金磊), Xiong-Yu Liang(梁熊玉), Jun-Qiang Li(李俊强), Xu-Yan Deng(邓绪彦), Jian-Yu Qin(秦建宇), Jia-Sen Zhang(张家森), and Li Yu(于丽)

Chin. Phys. B, 2024, 33 (**5**): 054210. DOI: 10.1088/1674-1056/ad2dca

## High-speed directly modulated distributed feedback laser based on detuned loading and photon-photon resonance effect

Yun-Shan Zhang(张云山), Yi-Fan Xu(徐逸帆), Ji-Lin Zheng(郑吉林), Lian-Yan Li(李连艳), Tao Fang(方涛), and Xiang-Fei Chen(陈向飞)

Chin. Phys. B, 2023, 32 (**9**): 094204. DOI: 10.1088/1674-1056/acc8c1

## Mode characteristics of VCSELs with different shape and size oxidation apertures

Xin-Yu Xie(谢新宇), Jian Li(李健), Xiao-Lang Qiu(邱小浪), Yong-Li Wang(王永丽), Chuan-Chuan Li(李川川), and Xin Wei(韦欣)

Chin. Phys. B, 2023, 32 (**4**): 044206. DOI: 10.1088/1674-1056/ac9821

## Broad bandwidth interference filter-stabilized external cavity diode laser with narrow linewidth below 100 kHz

Guan-Zhong Pan(潘冠中), Bao-Lu Guan(关宝璐), Chen Xu(徐晨), Peng-Tao Li(李鹏涛), Jia-Wei Yang(杨嘉炜), Zhen-Yang Liu(刘振杨)

Chin. Phys. B, 2018, 27 (**1**): 014204. DOI: 10.1088/1674-1056/27/1/014204

---

# An adjustment-free laser resonator based on micron-scale corner cube array

Pengyuan Chang(常鹏媛)[1], Xinrong Huang(黄欣荣)[1], Caolei Fu(傅曹雷)[1], Aiping Liu(刘爱萍)[1], Duo Pan(潘多)[2,†], Zhiyang Wang(王志洋)[2], and Jingbiao Chen(陈景标)[2,3]

[1] *Institute of Quantum Information and Technology, Nanjing University of Posts and Telecommunications, Nanjing* 210003, *China*
[2] *State Key Laboratory of Advanced Optical Communication Systems and Networks, Institute of Quantum Electronics, School of Electronics, Peking University, Beijing* 100087, *China*
[3] *Hefei National Laboratory, Hefei* 230088, *China*

(Received 20 October 2024; revised manuscript received 11 December 2024; accepted manuscript online 31 December 2024)

The topic of improving the mechanical stability of external cavity diode lasers (ECDLs) has recently attracted widespread attention and interest. The use of corner-cube-array (CCA)-based resonators provides a potential solution for this purpose, although continuous oscillation at super large incident angle remains challenging. In this work, we employ the CCA resonator to generate continuous oscillation within $\pm 20^\circ$ angular misalignment of cavity mirror in experiment. On the basis of retroreflection theory, the retroreflectivity of a CCA is analyzed by using optical simulation software. Notably, the experiment verifies the advantage of using a CCA over a plane mirror in laser resonator, thereby providing a promising approach for ECDLs. The threshold characteristic curves measured at different incident angles in the experiment verify that the CCA possesses an obvious anti-angle misalignment performance. This research introduces an alternative solution of using CCA resonator instead of parallel plane cavity, thereby realizing an adjustment-free ECDL with enhanced mechanical stability.

**Keywords:** laser resonant cavity, corner cube array, external cavity diode laser, threshold curve

**PACS:** 42.55.Px, 42.79.Bh, 42.15.Eq

**DOI:** 10.1088/1674-1056/ada434 **CSTR:** 32038.14.CPB.ada434

## 1. Introduction

Corner cube prisms, due to their excellent anti-angle misalignment and retroreflective properties, are widely used as retroreflectors in interferometers, communication links and lasers. As early as 1948, Peck reported on corner-cube-prism-based interferometers;[1] communication links utilizing corner cube prisms as backward reflectors extended the transmission distance from two meters[2] to hundreds of meters;[3] solid-state laser with 20° angular misalignment was achieved using a single corner cube prism as a cavity mirror;[4] and single-mode Faraday laser could have a substantial angular range $\pm 3^\circ$.[5] However, compared to large-size single corner cube prism, corner cube array (CCA) with enhanced retroreflectivity, quasi-phase conjugation, and compensation for wavefront distortions[6–8] has gradually replaced single corner cube prism in retroreflectors. Optimization of CCA structures, including tilt angles, joint configurations, corner cube sizes, and connection layer thicknesses, has significantly improved its optical performance, greatly enhancing its adaptability.[9–11] To date, numerous significant reports have documented the application of CCAs in fields such as space communication,[2,3,8] optoelectronic tracking,[12] lunar exploration,[13,14] traffic,[15,16] and lasers.[17] In space communication, the quasi-wavefront compensation effect of CCA effectively suppresses turbulence-induced attenuation, leading to better link performance.[8] In optoelectronic tracking, CCA with dihedral angle errors can achieve divergent reflected beams, forming uniform ring-shaped spots in the far field, thus enabling stable tracking of aerial moving platforms.[12,13] In lunar exploration, CCA plays a key role in tracking lunar landers and measuring Earth–Moon distances.[14] In traffic, CCA-based retroreflective sheeting is commonly used in guiding signs.[15,16] Additionally, since Barrett *et al.* reported on the quasi-phase conjugation characteristics of CCA in 1979,[7] which suppress wavefront distortions in optical systems, there has been increasing research on the application of CCA in lasers. For instance, CCA has been used to improve the beam qualities of solid-state thermal capacity lasers and a rubidium glass laser.[17]

However, in the field of lasers, external cavity diode laser (ECDL) and Fabry–Pérot (FP) cavity,[18] which rely on perfectly parallel front and rear cavity mirrors to achieve laser oscillation, present challenges such as complex mirror alignment processes and poor interference resistance.[19–22] For ECDLs, manual adjustment by visually observing the overlap between the reflected light from the cavity mirror and the laser source remains the basic method for aligning the external cavity. Over time, the cavity mirrors of ECDLs can become misaligned due

†Corresponding author. E-mail: panduo@pku.edu.cn

© 2025 Chinese Physical Society and IOP Publishing Ltd. All rights, including for text and data mining, AI training, and similar technologies, are reserved.

to mechanical deformation. Previous reports on adjustment-free lasers utilizing CCA with inner circle radius of each corner cube prism unit on the millimeter scale[17] did not verify their utility in high-precision ECDLs. Therefore, to address the issues of susceptibility to angular misalignment and complex mirror calibrating processes in high-precision ECDLs, CCA resonators urgently need to be developed.

In this work, we innovatively utilize micron-scale CCA to achieve adjustment-free and anti-angle misalignment ECDL. We demonstrate that the retroreflectivity of CCA is insensitive to the incident angle within a small range in simulations. Additionally, we make an ECDL based on a CCA resonator and achieve continuous oscillation within an incident angle range of $\pm 20^\circ$ at different cavity lengths. This is advantageous, as it simplifies the calibration process and enhances anti-angle misalignment. This development is significant for optimizing the stable performance of ECDLs, as it opens new possibilities for promising high-stability ECDLs and further advancements in ECDL technology.

## 2. Retroreflection simulation of CCA

### 2.1. Simulation model

Figure 1(a) shows the simulation model established using TracePro. Some simulation parameters for the CCA model are as follows: 1) the CCA consists of $24\times20$ corner cube prisms, each with a triangular bottom and a side length of 100 μm; 2) the surface reflectivity of the corner cube prism is 95%, and the mirror absorption is 5%; 3) each corner cube prism has three isosceles triangular surfaces perpendicular to each other and is arranged compactly with other prisms. Figure 1(b) illustrates a path of retroreflected light within a corner cube prism. When light enters normally from the ABC face, it undergoes four reflections, completing the direction vector reversal and forming retroreflected light. The shaded regions ($a$, $b$, and $c$) represent areas where light entering normally will not be retroreflected, referred to as ineffective retroreflection areas. The effective retroreflection area on the bottom surface of the corner cube prism is a blank area in the shape of a regular hexagon, occupying approximately $2/3$ of the bottom surface.[10,23]

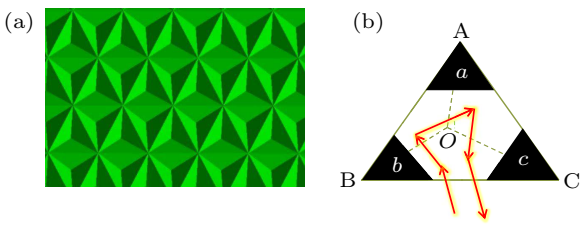



**Fig. 1.** (a) CCA simulation model. (b) Retroreflection process inside a single corner cube prism.

### 2.2. Analysis of CCA retroreflectivity

According to the standard Road Traffic Reflective Sheeting (GB/T 18833-2012), retroreflected light is defined as a light cone with its axis aligned in the reverse direction of the incident light and a half-angle width of 1°. While this definition is suitable for most scenarios, in laser applications, the reflected light must precisely align with the light source. Therefore, in the simulation, retroreflectivity $\theta$ is calculated by determining the ratio of the received luminous flux $\phi$ within the source area (a circle with radius of 0.7 mm) on the observation screen to the total luminous flux $\varphi$ emitted by the source. This can be expressed as

$$\rho = \frac{\phi}{\varphi}. \tag{1}$$

Figure 2(a) schematically illustrates the TracePro optical simulation system, which is positioned within a rectangular coordinate system defined by the $x$, $y$, and $z$ axes. The CCA is set in the $xoz$ plane. The simulated light source emits parallel light with a uniform spatial distribution and a waist of 0.6 mm in both the $X$ and $Y$ directions, following a Gaussian distribution in density. To enhance the clarity of the reflection traces, the observation screen is placed 20 mm away from the CCA, with the light source positioned 1 mm in front of the observation screen. Figures 2(b) and 2(d) display the reflection traces that occur when the CCA and a plane mirror are tilted at an angle of 33°. When the incident light reaches the CCA, two beams appear on the observation screen: one invalid reflection and one effective retroreflected beam that returns to the light source and illuminates the screen.

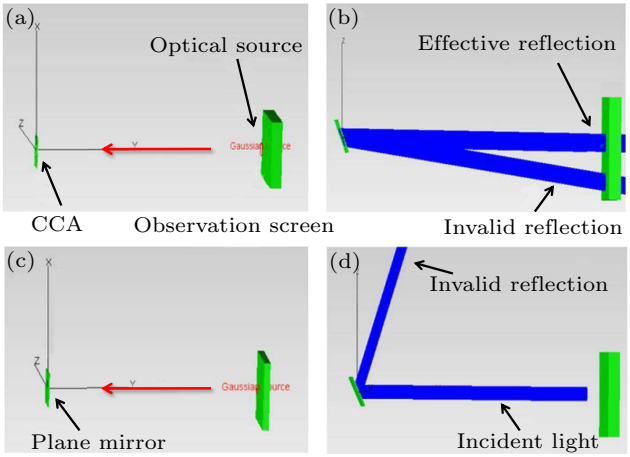



**Fig. 2.** Schematic of TracePro optical simulation system. (a) CCA optical simulation system design. (b) Reflection effect of CCA. (c) Plane mirror simulation system design. (d) Reflection effect of plane mirror.

In the optical simulation, we placed the CCA rotation pivot along the $x$-axis and rotated the optical simulation model around the origin of the coordinates. Ray tracing was performed while rotating the CCA in equal interval angles. Initially, the CCA was rotated from 0°, and the reflected patterns on the observation screen were recorded, as shown in

Fig. 3. Due to the Gaussian distribution of the source, the incident light is relatively concentrated, and the retroreflected beam distribution exhibits a similar characteristic. In Fig. 3(a), the retroreflected pattern appears with approximate hexagonal blanks, formed by the splicing together of shades, as illustrated in Fig. 1(b). As shown in Fig. 3(d), the reflected pattern nearly coincides with the retroreflected pattern on the observation screen. This occurs within a small angular range near 35°. Since such large-angle tuning is not required in ECDLs, the detailed causes of this phenomenon are not explored further in this work.

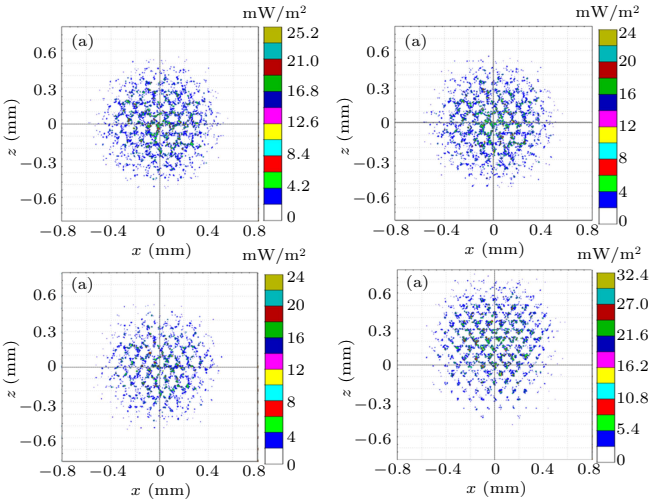



**Fig. 3.** Reflected patterns on observation screen. (a) 0°; (b) 10°; (c) 20°; (d) 35°. In (d), a reflected pattern overlapping with the retroreflected pattern, which occurs only when the rotation angle is near 35°.

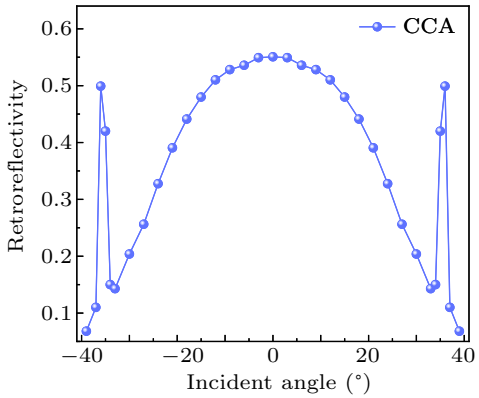



**Fig. 4.** The retroreflectivity as a function of the incident angle.

The ratio of the irradiance of the retroreflected light received within the source area to the incident light intensity is calculated as retroreflectivity, as shown in Fig. 4. It can be seen that the retroreflectivity of the CCA decreases as the rotation angle increases. This decrease occurs because the rotation of the CCA reduces the effective retroreflection area, thereby decreasing the flux of the retroreflected light. The changes in retroreflectivity can be neglected within a ±5° range, which may occur in ECDLs. When the rotation angle exceeds 40°, almost no patterns are found on the screen. Near 35°, a substantial increment in retroreflectivity is observed as the beam reflects back into the source area. As the rotation angle continues to increase, the reflected pattern moves out of the source area, and the retroreflectivity continues to decrease.

## 3. Experimental setup

### 3.1. CCA samples

In order to apply the CCA to ECDLs for anti-angle misalignment performance, we investigated retroreflective sheeting with a structure similar to the simulation model available on the market.[24–28] Ultimately, two samples were selected for experiments.

Both samples have microcrystalline corner cube structure that closely matches the simulation model. Unlike the simulation model, every single corner cube prism of the samples is solid filled with resin. Sample 1 is a microprism-type retroreflective sheeting, while sample 2 includes an added anti-aging layer. The scanning electron microscope (SEM) images of the reflective surface microstructures of samples 1 and 2 are shown in Figs. 5(a)–5(c) and 5(d)–5(f), respectively. The bottom edge length of each corner cube in sample 1 is approximately 170 μm, while sample 2 has the same microstructure with a bottom edge length of 120 μm. Due to the absence of an anti-aging layer in sample 1, its SEM images show more wear, leading to the selection of sample 2 for this experiment.

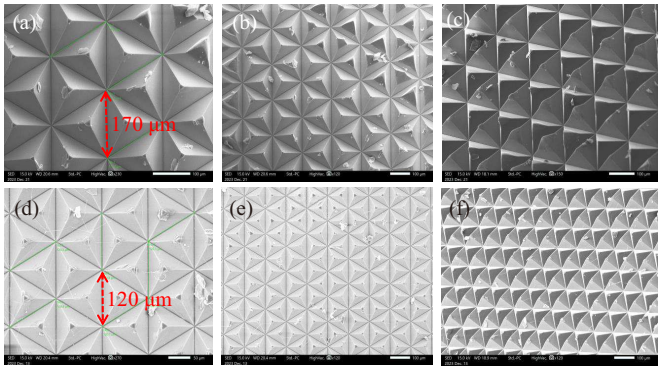



**Fig. 5.** SEM images of the CCA retroreflective sheeting samples. (a) Magnification (Mag) = 230, working distance (WD) = 20.6 mm; (b) Mag = 150, WD = 18.1 mm; (c) Mag = 230, WD = 20.6 mm; (d) Mag = 270, WD = 20.4 mm; (e) Mag = 120, WD = 20.4 mm; (f) Mag = 120, WD = 18.9 mm. Images (a)–(c) and (d)–(f) correspond to samples 1 and 2, respectively.

### 3.2. The ECDL based on CCA resonator

In order to achieve greater anti-angle misalignment, referred to as adjustment-free operation, we further investigated the CCA as a cavity mirror scheme. The experimental schematic and a photograph of the ECDL based on the CCA resonator are shown in Figs. 6(a) and 6(b). A 780 nm antireflection-coated laser diode (ARLD) serves as the gain medium, and the length of the CCA resonator is 10 cm with cavity mode spacing of 1.5 GHz. To simplify the experimental setup, no frequency-selective elements

are included in the external cavity. The light beam emitted by the ARLD passes through a half-wave plate (HW) and a polarization beam splitter (PBS). By adjusting the HW and PBS, we set the power proportion of the transmitted and reflected beams as 6:4. As shown in Fig. 6(a), the selected CCA sample is positioned along the direction of light propagation and fixed on a high-precision rotary table (Thorlabs, PR01M). The beam reaching the CCA is then retroreflected back to the PBS, with the transmitted light (P-polarized light) feedback to the ARLD and reflected light (S-polarized light) output. The laser after oscillation is detected by a power meter (PM) and optical beam profiler (OBP). Simultaneously, we record the retroreflected patterns on the opposite side of the PM. The rotation pivot is coplanar with the reflective surface, ensuring that continuous rotation of the CCA can tilt the angle of the light beam while maintaining a constant cavity length.

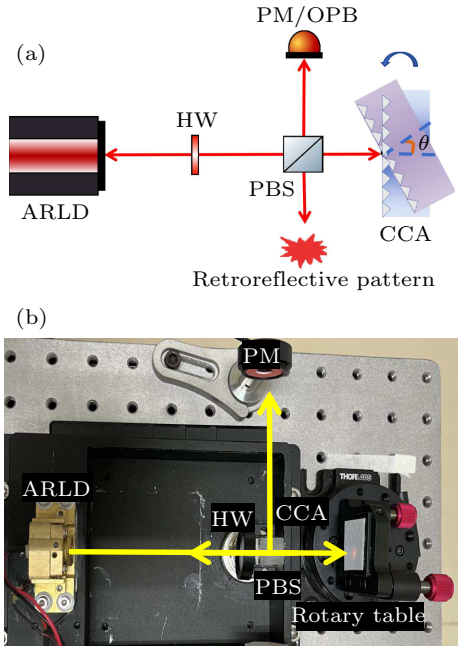



**Fig. 6.** (a) Schematic of an ECDL based on CCA resonator; ARLD, antireflection-coated laser diode; HW, half-wave plate; PBS, polarization beam splitter; PM, power meter; OBP, optical beam profiler; CCA, corner cube array. (b) Photograph of CCA resonator experimental setup.

## 4. Experimental results

### 4.1. Laser beam profile with CCA resonator

When the light was incident perpendicularly to the CCA, the retroreflected patterns instead of the laser output spot were recorded in Figs. 6(a)–6(f), with the light density centered within 1 cm. It is evident that there is a six-direction divergence and a dark fringe in the horizontal direction. The divergence is primarily due to the inherent structure of the CCA, while the cause of the fringe remains unknown and requires further exploration. Since the cavity mirror area at the rear end of the ARLD is extremely small, the pattern has minimal impact on beam quality, with only the fundamental mode contributing to the external cavity feedback.

Additionally, as shown in Figs. 7(g)–7(i), we measured the laser beam profile using OBP. This confirms that the intensity of the laser after oscillation is primarily distributed in the fundamental Gaussian mode ($TEM_{00}$) and presents good beam quality, with a beam width clip of 13.5% in the $X$ direction of 2662 μm and 1298 μm in the $Y$ direction, and a beam quality factor $M^2$ of less than 1.1.

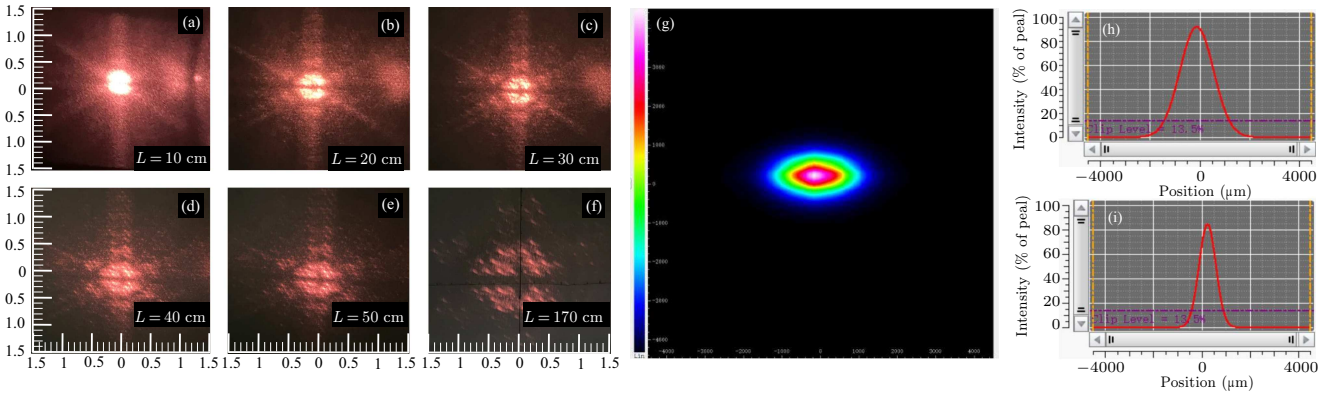



**Fig. 7.** The photograph of retroreflected patterns from the CCA (a)–(f) with different distances of 10 cm, 20 cm, 30 cm, 40 cm, 50 cm, and 170 cm, respectively. The transverse spatial profile of the laser beam is presented in (g)–(i). Here, (h) and (i) represent the Gaussian fitted curves in horizontal and vertical directions, respectively.

### 4.2. Threshold characteristics at different cavity lengths

Threshold current is the most crucial and basic parameter to characterize a diode laser.[29,30] The effective laser oscillation of an ECDL depends on the laser gain and the losses arising from light going through or diffracting at the reflection mirrors, and scattering or absorption within an active light-emitting medium during one round trip in the resonator. The driving current strengthens the gain, and when the gain and losses are balanced, the current is referred to as the threshold current ($I_{th}$). At low driving currents, the ECDL behaves like a light-emitting device where the carrier density in the diode is insufficient for population inversion; spontaneous

emission dominates in this region. As the driving current exceeds the threshold current, population inversion occurs, stimulated emission becomes predominant, and the slope of the power–current (*P–I*) curve increases.

Figure 8(a) illustrates the *P–I* curves for different cavity lengths when the cavity mirror is a high-reflectivity plane mirror (with reflectivity higher than 99%) at 780 nm. The data indicates that for a parallel plane cavity, the threshold current increases with longer cavity lengths, primarily due to insufficient beam collimation. Figure 8(a) shows that the maximum power of parallel-plane-cavity laser is 7.55 mW at an injection current of 170 mA, and the threshold current and slope efficiency are 90 mA and 0.1 mW/mA, respectively.

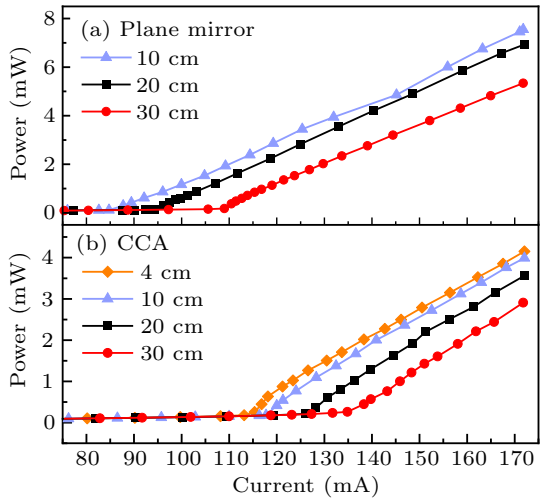



**Fig. 8.** (a) The *P–I* curves of parallel plane cavity with different cavity lengths; (b) *P–I* curves of CCA resonator with different cavity lengths. The diamond, triangle, square, and circular dotted lines represent the cavity lengths of 4 cm, 10 cm, 20 cm, and 30 cm, respectively.

To analyze the threshold characteristics of the CCA resonator at different cavity lengths, we changed the cavity length and set the angle of the high-precision rotary stable at 0°. Figure 8(b) shows the *P–I* curves for different cavity lengths when the cavity mirror is the CCA. Compared to the former, the threshold current increases and the maximum power decreases.

Table 1 presents the threshold currents and maximum powers for different cavity lengths. The maximum power (MP) for a cavity length of 10 cm in the parallel plane cavity serves as the reference, and the normalized maximum powers for other conditions are derived accordingly. From Table 1, it is evident that for both types of cavity mirrors, as the cavity length increases, the threshold current also increases while the maximum power decreases. However, the threshold current of the CCA resonator is generally higher than that of the parallel plane cavity. This can be attributed to the divergence of reflected light resulting from the CCA structure and the retroreflectivity. Additionally, simulation results indicate that for a CCA model with 95% reflectivity, the retroreflectivity is less than 60%, and part of the beam retroreflected from the CCA output from the PBS due to the polarization characteristics are altered. Thus, the feedback efficiency is lower than that of the parallel plane cavity. However, current coating technology can achieve higher retroreflectivity for CCA, thereby improving feedback efficiency.[10] Furthermore, when comparing the normalized maximum power, it is evident that the maximum power of the CCA resonator is nearly half that of the parallel plane cavity at the same cavity lengths. Therefore, appropriate cavity lengths must be matched to achieve larger laser output power. Besides, optimizing the structure can reduce divergence angles, thereby improving feedback efficiency.

**Table 1.** Threshold characteristics of parallel plane cavity and CCA resonator with different cavity lengths.

| Type of cavity mirror | Length (cm) | $I_{th}$ (mA) | MP (mW) | Normalization |
|---|---|---|---|---|
| Plane mirror | 10 | 87.73 | 7.553 | 100% |
| Plane mirror | 20 | 96.28 | 6.934 | 91.80% |
| Plane mirror | 30 | 110.45 | 5.337 | 70.66% |
| CCA | 4 | 115.34 | 4.152 | 54.97% |
| CCA | 10 | 117.75 | 3.992 | 52.85% |
| CCA | 20 | 126.09 | 3.563 | 47.17% |
| CCA | 30 | 134.85 | 2.910 | 38.52% |

### 4.3. Threshold characteristics at different incident angles

To analyze the effect of incident angle on threshold characteristics, the CCA was continuously rotated during the experiment, and the laser maintained continuous oscillation output within incident angles of approximately ±20°. Figure 9 illustrates the experimental results, showing the output power of a typical dotted line in the CCA resonator as a function of drive current, under rotation angles of 0° and 20° in both clockwise and counterclockwise directions. It can be observed that the laser operated normally, with a slight increase in threshold current at an incident angle of ±20°. Compared to our previous work of using a single large-size corner cube reflector (Thorlabs, HHR1272-M03) to achieve ±3° angular misalignment,[5] the CCA has better anti-angle misalignment performance.

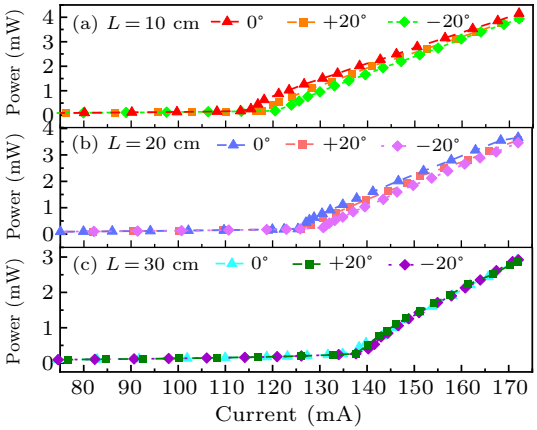



**Fig. 9.** The *P–I* curves of CCA resonator at different incident angles. (a) Cavity length 10 cm; (b) cavity length 20 cm; (c) cavity length 30 cm. The triangle, square and diamond dotted line represent the incident angles of 0°, +20° and −20°.

Table 2 demonstrates the effect of incident angle on the threshold characteristics of the CCA resonator. When the CCA is tilted at 20°, the threshold current increases, which can be attributed to the reduced feedback efficiency. Under a cavity length of 10 cm, comparing the incident angles of +20° and −20°, differences in $I_{th}$ and the slope of the *P*–*I* curves are primarily caused by measurement errors and system mechanical instability. However, under the same cavity length, the 20° tilt angle has only a minor effect on the threshold characteristics of the CCA.

**Table 2.** Threshold characteristics of CCA resonator with different cavity lengths.

| Length (cm) | Incident angle (°) | $I_{th}$ (mA) | MP (mW) | Normalization |
|---|---|---|---|---|
| 10 | 0 | 117.75 | 3.992 | 100% |
| 10 | +20 | 125.85 | 5.007 | 125.42% |
| 10 | –20 | 120.47 | 3.935 | 98.57% |
| 20 | 0 | 123.09 | 3.563 | 89.25% |
| 20 | +20 | 125.36 | 3.453 | 86.50% |
| 20 | –20 | 125.85 | 3.461 | 86.70% |
| 30 | 0 | 134.85 | 2.910 | 72.90% |
| 30 | +20 | 137.66 | 2.922 | 73.20% |
| 30 | –20 | 137.58 | 2.874 | 71.99% |

## 5. Conclusion and perspectives

In conclusion, we have developed a novel adjustment-free ECDL based on CCA resonator. The angular insensitivity of the CCA allows us to overcome the issue of angular misalignment. With the optical simulation, we obtain the retroreflectivity as function of the incident angle. The simulation results show that the retroreflectivity changes negligibly within a small angular range of ±5°, which verifies its anti-angle misalignment performance in CCA resonator. In the CCA resonator, the beam quality is good with a distribution of fundamental Gaussian mode ($TEM_{00}$). In addition, we experimentally measure the *P*–*I* curves in different cavity lengths and a large angle misalignment ±20°. It shows that the CCA resonator can still maintain continuous oscillation at large angular misalignment, thereby bringing considerable convenience to the operation of laser resonator and improving the mechanical stability of ECDLs. Furthermore, the successful implementation of the CCA resonator not only illustrates the potential applications of CCA in laser resonators but also provides practical references for the design and improvement of ECDLs.

## Acknowledgements

The present work was supported by the Natural Science Foundation of Jiangsu Province (Grant No. BK20240613), Jiangsu Province's "Innovation and Entrepreneurship Doctor" Program (Grant No. JSSCBS20230088), Natural Science Foundation of Nanjing University of Posts and Telecommunications (Grant No. NY224123), Natural Science Research Start-up Foundation of Recruiting Talents of Nanjing University of Posts and Telecommunications (Grant No. NY222112), Beijing Nova Program (Grant No. 20240484696), Wenzhou Major Science and Technology Innovation Key Project (Grant No. ZG2020046), and INNOVATION Program for Quantum Science and Technology (Grant No. 2021ZD0303200).

## References

[1] Peck E R 1948 *JOSA* **38** 1015
[2] Chu P B, Lo N R, Berg E C and Pister K S J 1997 *Proceedings IEEE The Tenth Annual International Workshop on Micro Electro Mechanical Systems*, January 26–30 1997, Nagoya, Japan, IEEE, p. 350
[3] Zhou L X, Kahn J M and Pister K S J 2003 *J. Microelectromech. Syst.* **12** 233
[4] Cheng Y, Wang X B, Sun B and Mao S Q 2000 *Chin. J. Lasers* **27** 537 (in Chinese)
[5] Wang Z Y, Liu Z J, Miao J X, Shi H B, Qin X M, Guan X L, Zhang J, Chang P Y, Shi T T and Chen J B 2024 *IEEE Photonics J.* **16** 1502809
[6] Zhang X N, Shen M J and Wang W W 2016 *Opt. Instrum.* **38** 69 (in Chinese)
[7] Barrett H H and Jacobs S F 1979 *Opt. Lett.* **4** 190
[8] Yang G W, Zhang J W, Zhang J J, Bi M H, Chen T N, You S Z, Zhou X F, Wang T S, Li J and Geng H J 2020 *J. Lightwave Technol.* **39** 1355
[9] Lou Y M, Wang H, Liu Q K, Shi Y C and He S L 2010 *Appl. Opt.* **49** 5567
[10] Pi J and Shang K 2014 *Acta Photon. Sin.* **43** 0423003 (in Chinese)
[11] Yang G, Duan M H, Li Z Z and Chen J H 2022 *Laser Optoelectron. Prog.* **59** 1308002 (in Chinese)
[12] Zhou X F, Qi Z M, Luo X Q, Liu C A, Zhu J H, Wang Z H, Zhang Y and Zi Y Y 2016 *Acta Phys. Sin.* **66** 084201 (in Chinese)
[13] Degnan J J 2023 *Photonics* **10** 1215
[14] He Y, Liu Q, He J J, Li M, Duan H Z, Ye X J and Luo J 2018 *Chin. Phys. B* **27** 100701
[15] Fan W, Zeng J, Gan Q Q, Ji D X, Song H M, Liu W Z, Shi L and Wu L M 2019 *Sci. Adv.* **5** eaaw8755
[16] Qi Y, Zhou C T, Niu W B, Zhang S F, Wu S L, Ma W and Tang B T 2020 *Adv. Opt. Mater.* **8** 2001367
[17] Liu W B, Zhong M, Xia H J and Wen Y 2011 *Laser Technol.* **35** 745 (in Chinese)
[18] Lv Y S, Xie P H, Xu J, Li Y T and Zhang H R 2024 *Chin. Phys. B* **33** 014210
[19] Chang P Y, Chen Y L, Shang H S, Guan X L, Guo H, Chen J B and Luo B 2019 *Appl. Phys. B* **12** 230
[20] Chang P Y, Peng H F, Zhang S N, Chen Z Y, Luo B, Chen J B and Guo H 2017 *Sci. Rep.* **7** 8995
[21] Baillard X, Gauguet X, Bize S, Lemonde P, Laurent P, Clairon A and Rosenbusch P 2006 *Opt. Commun.* **266** 609
[22] Thompson D J and Scholten R E 2012 *Rev. Sci. Instrum.* **83** 023107
[23] Eckhardt H 1971 *Appl. Opt.* **10** 1559
[24] Lin J Z and Lin J Z (China Patent) CN202210237359.5 [2022-12-07]
[25] Xu M Q, Liang G D and Xu J C (China Patent) CN201711432626.X [2018-12-05]
[26] Lu Y J, Ran K and Wang Y T (China Patent) CN201410823342.3 [2017-01-25]
[27] Lv L, Liu M X and Chui X Y (China Patent) CN202011322105.0 [2021-12-02]
[28] Chen H B (China Patent) CN201910357893.8 [2021-12-04]
[29] Ye C Y 2004 *Tunable External Cavity Diode Lasers* (Singapore: World Scientific)
[30] Su C B and Olshansky R 1983 *Appl. Phys. Lett.* **43** 856